Neural Comput & Applic
DOI 10.1007/s00521-014-1795-6

ORIGINAL ARTICLE

Parameter extraction of solar cell models using chaotic asexual reproduction optimization

Xiaofang Yuan · Yuqing He · Liangjiang Liu

Received: 2 June 2014 / Accepted: 9 December 2014

Abstract To simulate solar cell systems or to optimize photovoltaic (PV) system performance, the estimation of solar cell model parameters is extremely crucial. In this paper, the parameter extraction of solar cell models is formalized as a multi-dimensional optimization problem, and an objective function is established minimizing the errors between the estimated and measured data. A novel chaotic asexual reproduction optimization (CARO) using chaotic sequence for global search is applied to this parameter extraction problem. All the seven or five parameters of solar cell models are extracted simultaneously using measured input–output data. The CARO has been tested with different solar cell models, i.e., double diode, single diode, and PV module. Comparison simulation results with other parameter extraction techniques show that the CARO signifies its potential as another optional method.

Keywords Parameter extraction · Solar cell models · Chaotic asexual reproduction optimization (CARO) · Chaotic sequence

1 Introduction

Solar energy is one of the most promising renewable energy sources world widely utilized due to readily available all over the world, easy installation, low maintenance, and almost zero pollution [1–4]. With the increasing utilization of solar energy, the modeling of photovoltaic (PV) generation system has received significant attention [1–6]. Usually, a PV generation system includes various sizes [5]: solar cell, PV module and PV array. To simulate solar cell systems or to optimize PV systems performance, the estimation of solar cell model parameters is extremely crucial.

In the last years, various parameters extraction techniques have been applied in this field, they are as follows: (1) least-squares method (LSM)-based nonlinear fitting algorithm [7, 8], the major defect of LSM fitting algorithm is its sensitivity to outliers. Outliers usually have a great impact on the LSM fitting performance because the effect of these extreme data points is magnified by squaring the residuals. (2) two types of analytical solution methods [9–16]: one type is approximate analytical methods [9–11] which are commonly expressed in terms of elementary functions, the other type is exact analytical methods [12–16] based on the Lambert W-function which cannot be expressed in terms of elementary functions. However, the accuracy of analytical solution methods is at the cost of computation speed. Moreover, analytical solution methods have poor robustness as they are greatly influenced by measurement noise. (3) artificial neural network (ANN)-based intelligent modeling techniques [17–21]. Intelligent modeling techniques bring several benefits, such as requiring less historical measured data, arbitrary nonlinear function approximation capability. Shortcomings in intelligent modeling techniques include dependence on model structure and learning algorithm, long training times, proneness to over-fitting. (4) Meta-heuristics and optimization algorithms, such as genetic algorithm (GA) [22], particle swarm optimization (PSO) [23, 24], pattern search

X. Yuan (✉) · Y. He
College of Electrical and Information Engineering, Hunan University, Hunan 410082, China
e-mail: yuanxiaofang126@126.com

L. Liu
Hunan Institute of Metrology and Test, Changsha 410014, China

Published online: 24 December 2014

(PS) [25, 26], differential evolution (DE) [27], simulated annealing (SA) [28], and artificial bee swarm optimization (ABSO) [29] so on. However, the performance of these optimization algorithms relies strongly on their search capability, which commonly requires a good balance between exploration and exploitation.

In view of the limitations of the former parameters extraction techniques, this paper proposes a novel chaotic asexual reproduction optimization (CARO) for this parameter extraction problem. Asexual reproduction optimization (ARO) [30–33] is a kind of biologically inspired optimization technique which has been proposed recently. Some characteristics of the ARO include but are not limited to the fast convergence time, no parameter setting, being model free and biological foundations [30–33]. However, genetic diversity of ARO becomes very low as it is an individual-based algorithm; in addition, ARO has poor adaptation ability with the turbulent environment. In view the limitation of original ARO, chaotic sequence is applied to ARO to propose a novel CARO in this paper. In the CARO, chaotic sequence with global exploration capacity is employed in the reproduction procedure. Consequently, a good balance between exploration and exploitation can be achieved in the CARO. The parameter extraction of solar cell models is formalized as a multi-dimensional optimization problem, and an objective function is established minimizing the errors between the estimated and measured data. All the seven or five parameters of solar cell models are extracted simultaneously using measured input–output data. The proposed CARO-based parameter extraction technique has been tested with different solar cell models, i.e., double diode, single diode, and PV module.

The rest of this article is arranged as follows. The parameters extraction problem of solar cell models is introduced in Sect. 2. Section 3 gives presentation of the proposed CARO technique. Comparison simulations have been used to verify the performance of CARO for solar cell models in Sect. 4. Conclusions are presented in Sect. 5.

2 Problem formulation

Although various equivalent circuit models have been developed to describe the behavior of solar cell, in practice, there are two commonly used solar cell models: the double and single diode models.

2.1 Double diode model

The equivalent circuit of a double diode model is illustrated in Fig. 1a. In the double diode model, the cell terminal current I_t is usually formulated as follows [5]:

$$I_t = I_{ph} - I_{d1} - I_{d2} - I_{sh} \tag{1}$$

where I_{ph} is the photo-generated current; I_{d1} and I_{d2} denote the first and second diode current, respectively; I_{sh} denotes the shunt resistor current.

Currents I_{d1}, I_{d2} and I_{sh} can be specifically represented according to Shockley equation, as a result, Eq. (1) is rewritten as follows [5, 6, 25]:

$$\begin{aligned} I_t = I_{ph} &- I_{sd1}\left[\exp\left(\frac{q(V_t + R_s I_t)}{n_1 kT}\right) - 1\right] \\ &- I_{sd2}\left[\exp\left(\frac{q(V_t + R_s I_t)}{n_2 kT}\right) - 1\right] - \frac{V_t + R_s I_t}{R_{sh}} \end{aligned} \tag{2}$$

where V_t is the terminal voltage; I_{sd1} and I_{sd2} are the diffusion and saturation currents, respectively; R_s and R_{sh} are the series and shunt resistances, respectively; n_1 and n_2 are the diffusion and recombination diode ideality factors; q denotes the electronic charge (1.6×10^{-19} C), k denotes the Boltzmann constant (1.38×10^{-23} J/K), and T denotes the cell temperature (K). Given a set of measured V–I data for such double diode model in Eq. (2), we can see that seven parameters are unknown, they are, $R_s, R_{sh}, I_{ph}, I_{sd1}, I_{sd2}, n_1$ and n_2. For different solar cells, these unknown parameters are varied.

2.2 Single diode model

The equivalent circuit of a single diode model is illustrated in Fig. 1b. In the single diode model, with the use of non-physical diode ideality factor n, the diffusion and recombination currents are combined together.

For such a single diode model, Eq. (2) is changed to the following from as [5, 6, 25]:

$$I_t = I_{ph} - I_{sd}\left[\exp\left(\frac{q(V_t + R_s I_t)}{nkT}\right) - 1\right] - \frac{V_t + R_s I_t}{R_{sh}} \tag{3}$$

Given a set of measured V–I data, the parameter extraction problem for such a single diode model in Eq. (3) reduces to find five unknown parameters, they are, $R_s, R_{sh}, I_{ph}, I_{sd}$, and n.

2.3 PV module model

A typical model structure of a PV module (using single diode model) is illustrated in Fig. 2, which is effectively the interconnection of solar cells in series or/and parallel ($N_s \times N_p$) configuration. The output current equation of a PV module is mathematically expressed as in the following equation [27, 28]:

$$I_t = I_{ph} N_p - I_{sd} N_p\left[\exp\left(\frac{q(\frac{V_t}{N_s} + I_t \frac{R_s}{N_p})}{nkT}\right) - 1\right] - \frac{\frac{V_t N_p}{N_s} + R_s I_t}{R_{sh}} \tag{4}$$

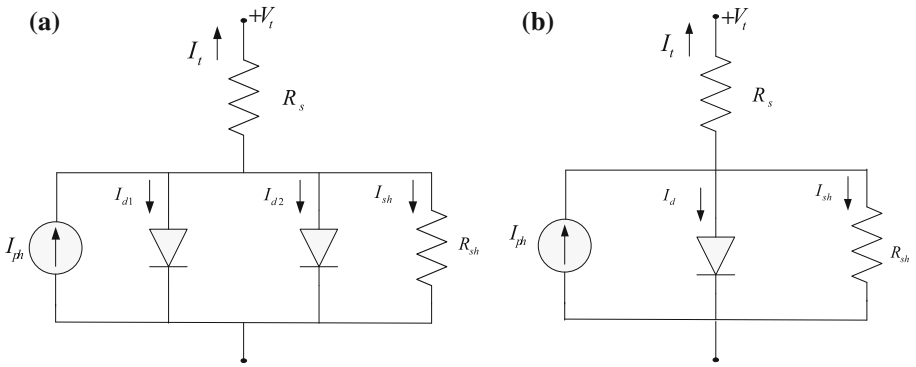

Fig. 1 Equivalent circuit of solar cell models. **a** Double diode model, **b** single diode model

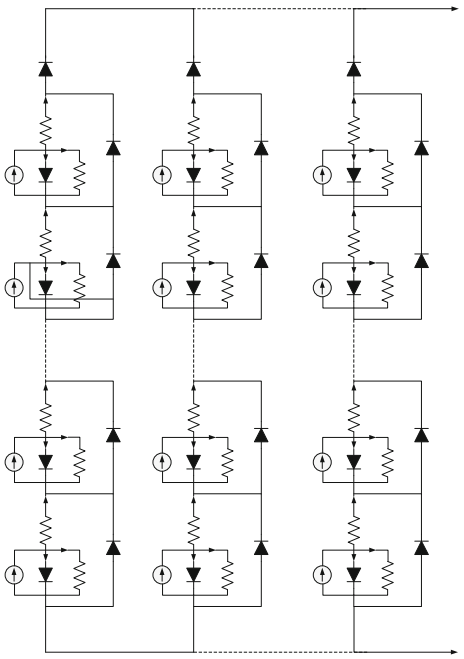

Fig. 2 Equivalent circuit model of a PV module

As this PV module comprises of series and parallel combinations using single diode model, five unknown parameters ($R_s, R_{sh}, I_{ph}, I_{sd}$ and n) are need to be extracted as in Eq. (3).

2.4 Optimization problem in parameter extraction of solar cell models

In this paper, the parameter extraction of solar cell models is posed as an optimization process which makes the difference minimum between the real data and estimated values. This optimization process is similar to meta-heuristics and optimization algorithms-based solar cell models parameters extraction techniques [22–29]. The optimization process is typically implemented in the following way: a set of real *V–I* data of solar cell or PV module is measured, an objective function minimizing the difference between the real data and estimated values is defined, then an optimization algorithm is applied to tune the parameters until the best objective function obtained. After the optimization procedure, the best solutions obtained by the optimization algorithm is just the extracted optimal parameters values.

Each solution of this parameter extraction problem is given by a vector X, where $X = [R_s \quad R_{sh} \quad I_{ph} \quad I_{sd1} \quad I_{sd2} \quad n_1 \quad n_2]$ and $X = [R_s \quad R_{sh} \quad I_{ph} \quad I_{sd} \quad n]$ are for the double and single diode model, respectively. For this optimization problem, an objective function needs to be defined. To define the objective function for solar cell models parameters extraction, Eqs. (2)–(4) are rewritten in their homogeneous forms as follows:

$$f(V_t, I_t, X) = I_t - I_{ph} + I_{sd1}\left[\exp\left(\frac{q(V_t + R_s I_t)}{n_1 kT}\right) - 1\right] + I_{sd2}\left[\exp\left(\frac{q(V_t + R_s I_t)}{n_2 kT}\right) - 1\right] + \frac{V_t + R_s I_t}{R_{sh}} \tag{5}$$

$$f(V_t, I_t, X) = I_t - I_{ph} + I_{sd}\left[\exp\left(\frac{q(V_t + R_s I_t)}{nkT}\right) - 1\right] + \frac{V_t + R_s I_t}{R_{sh}} \tag{6}$$

$$f(V_t, I_t, X) = I_t - I_{ph}N_p + I_{sd}N_p\left[\exp\left(\frac{q(\frac{V_t}{N_s} + I_t\frac{R_s}{N_p})}{nkT}\right) - 1\right] + \frac{\frac{V_t N_p}{N_s} + R_s I_t}{R_{sh}} \tag{7}$$

When different solutions X are put into Eqs. (5)–(7), the calculated $f(V_t, I_t, X)$ for each pair of *V–I* data is usually different. In most cases, the root-mean-square error (RMSE) is a criterion to evaluate the difference between the real data and estimated values. Therefore, the following objective function to minimize RMSE is employed in this paper for parameters extraction of solar cell models:

$$\text{Minimize} \quad \text{RMSE} = \sqrt{\frac{1}{M}\sum_{i=1}^{M} f(V_t, I_t, X)^2} \tag{8}$$

where M is the number of real V–I data. The parameters extraction error will result in a nonzero objective function RMSE, which is used to guide the optimization algorithm for better parameters vector X. If calculated RMSE is bad, the parameters vector X are tuned by the optimization algorithm and sent to Eqs. (5)–(7) again. This iterative procedure for improving the parameters vector X is usually stopped when the objective function is good enough or the optimization algorithm has reached the maximum number of iteration.

3 CARO technique

3.1 Standard ARO technique

Generally speaking, biological reproduction in nature includes two kind of reproduction: sexual and asexual reproduction. Sexual reproduction is a process that creates a new organism by combining the genetic material of two organisms. Sexual reproduction is the primary method of reproduction for the vast majority of macroscopic organisms, including almost all animals and plants [30, 31]. Asexual reproduction is another mode of reproduction by which offspring arise from a single organism and inherit the genes of that parent only. Asexual reproduction is also used by many plants, e.g. spider plants, bacteria, hydra, yeast, and jellyfish. Although they do not sexually reproduce, there are ways, like budding and gemmules, in which genes get transferred between asexual individuals. Asexual reproduction has rapid population growth in stable environments and it requires less energy. The disadvantage of strictly asexual reproduction is that genetic variability decreases, and the population is less able to survive changing environments [31].

The asexual reproduction optimization(ARO) [30–33] is a novel kind of individual-based optimization algorithm, which models the budding mechanism of asexual reproduction. In the ARO, a parent produces a bud through a reproduction operator; thereafter, the parent and its bud compete to survive according to a fitness designed for the underlying objective function of optimization problem [32]. The ARO may effectively explore the search space and exploit from available information, and some characteristics of ARO include but are not limited to the fast convergence time, no parameter setting, being model free and biological foundations [30, 31].

The optimization problem is specified as follows:

$$Minimize \quad f(X) \quad subject \quad to \quad X \in [L, U] \tag{9}$$

where $f(X)$ is an objective function; $X = (x_1, x_2, \ldots, x_n)$ is the set of each decision variable; n is the number of decision variables; L and U are the lower and upper bounds for decision variable X.

Table 1 illustrates the pseudo code of standard ARO technique. To start the ARO technique, an individual (parent) is first generated randomly between the lower and upper bounds, then the offspring (*bud*) is produced through a mechanism called reproduction. Thereafter, the parent and its offspring compete to survive according to an objective function or a fitness function. If the parent has better fitness and wins the competition, the offspring (*bud*) will be discarded totally and vice versa. The ARO technique repeats steps described in Table 1 until the stopping conditions are met.

In ARO technique, the reproduction of the *bud* is the key step for both exploration and exploitation. Generally, the reproduction of the *bud* includes two main steps: mutation operation and merging operation. Now, we will describe the reproduction of the *bud* for binary encoding and real number encoding.

In the binary encoding of ARO, each individual is represented by a binary string. The reproduction mechanism in binary encoding (i.e., bit strings) is illustrated in Fig. 3.

Table 1 Algorithmic description of ARO technique

```
Begin
   k = 1;
   Parent(k) = Initialize (L,U);          % Parent(k) initialization between lower and upper bound
   Fit_Parent(k) = fitness(Parent(k));    % Fitness of Parent(k) is calculated
   while stopping conditions are not met  % Stopping criteria
      Bud(k) = Reproduce(Parent(k));      % Parent(k) reproduces a Bud(k)
      Fit_Bud(k) = fitness(Bud(k));       % Fitness of Bud(k) is calculated
      if Fit_Bud(k) is better than Fit_Parent(k)   % Bud(k) is better than Parent(k)
      Parent(k) = Bud(k);                 % Bud(k) is replaced with Parent(k)
     else
      Clear Bud(k);                       % Bud(k) is discarded
      end
      k= k + 1;
   end while
End
```

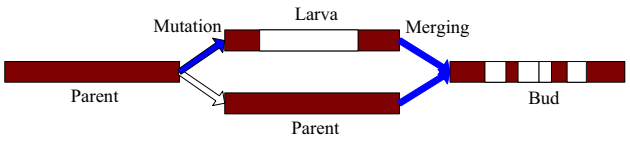

Fig. 3 The ARO reproduction mechanism

The first step of reproduction is mutation operation, a substring of length g bits uniformly distributed in $[1, Length]$, $g \sim Uniform\,[1, Length]$, is randomly selected for each chromosome. The *Length* denotes the length of a chromosome. Subsequently, 1's in this segment of bits are replaced by 0 and vice versa; i.e., the bits in the substring mutate. The second step of reproduction is the merging operation; therefore, the parent and its offspring can share their information by merging. In other words, during the merging process, the crossover implicitly takes place.

In addition to binary encoding, real number encoding is also considered in ARO technique. The reproduction of the *bud* in real number representation can be described by:

$$X'_{\mathrm{k}} = Y_{\mathrm{k}} + \gamma, \quad \gamma \sim U[-a, a] \tag{10}$$

$$X_{\mathrm{k}} = \alpha X'_{\mathrm{k}} + (1-\alpha) Y_{\mathrm{k}} \tag{11}$$

where Y_{k} and X_{k} are the parent and the offspring at kth generation, respectively; $\gamma \sim U[-a, a]$ is uniform random mutation; $\alpha X'_{\mathrm{k}} + (1-\alpha) Y_{\mathrm{k}}$ is arithmetic merging with $\alpha \in [0, 1]$.

After reproduction, the fitness of the bud is computed according to the objective function. As shown in Table 1, the fitness of the bud is compared with that of the parent. Therefore, the most deserved individual will survive and it is permitted to reproduce. The competitive selection of the parent and the offspring at kth generation is given by:

$$Y_{\mathrm{k+1}} = \begin{cases} X_{\mathrm{k}}, & \text{if } f(X_{\mathrm{k}}) < f(Y_{\mathrm{k}}) \\ Y_{\mathrm{k}}, & \text{otherwise} \end{cases} \tag{12}$$

The genetic diversity of ARO becomes very low as it is an individual-based algorithm, so it is not easy for ARO to reach global solution especially for multi-model problems. Furthermore, individual-based ARO has poor adaptation ability with the turbulent environment. When ARO starts from a bad initial point, it is very hard to find a good solution.

3.2 Proposed CARO technique

Due to the non-repetition of chaos, chaotic sequence carries out overall search at higher speed than stochastic ergodic search that depends on the probabilities [34, 35]. Notably, a lot of existing optimization results demonstrated that chaotic sequences escape from local minima more easily than evolutionary algorithms including GA, SA, PSO, ACO, and DE so on [36]. Recently, chaos has been successfully applied to improve global search ability of optimization algorithms, such as chaotic particle swarm optimization [24, 35], chaotic genetic algorithms [37], chaotic ant swarm optimization [38], chaos gravitational search algorithm [39], chaotic harmony search algorithm [40], chaos embedded great deluge algorithm [41], etc. The simulations in these literatures [24, 35, 37–41] have shown solutions diversity and global optimization capacity of chaos-based optimization algorithms.

In this section, chaos will be applied to ARO technique in real number encoding, and a novel chaotic ARO (CARO) is proposed in this paper. Several improvements in the CARO are considered as follows:

(a) As the disadvantage of asexual reproduction is that genetic variability decreases, and the ARO technique is easy to converge to local optimal. In view of the limitation of ARO, here the mutation operation of CARO technique is changed to:

When iteration number $k \le k_1$ (k_1 is a positive number), the CARO technique will search the total decision variable space for exploration as follows:

$$X'_{\mathrm{k}} = Y_{\mathrm{k}} + S_1(\cdot) \cdot \max\{U - Y_{\mathrm{k}}, Y_{\mathrm{k}} - L\} \tag{13}$$

where $max\{U - Y_{\mathrm{k}}, Y_{\mathrm{k}} - L\}$ means the maximum between $(U - Y_{\mathrm{k}})$ and $(Y_{\mathrm{k}} - L)$; $[L, U]$ means the search space of decision variables; $S_1(\cdot)$ is the chaotic sequence like iterative chaotic map with infinite collapses (ICMIC) [41]:

$$r_{\mathrm{k+1}} = S_1(r_{\mathrm{k}}) = \sin\left(\frac{20}{r_{\mathrm{k}}}\right), \quad k = 1, 2, 3, \ldots \tag{14}$$

When $k > k_1$, the search space will be shrunk according to the iteration number, this may be effective for exploitation as:

$$X'_{\mathrm{k}} = Y_{\mathrm{k}} + S_1(\cdot) \cdot \frac{U - L}{2} \cdot \left(\frac{k_{\max} - k}{k_{\max}}\right)^2 \tag{15}$$

where $k_{\max}$ is the maximum number of iteration.

It can be seen from Eqs. (13) and (15) that the exploration is emphasized at the early search process ($k \le k_1$) while the exploitation is emphasized at the later search process ($k > k_1$).

(b) In the merging operation of ARO as in Eq. (11), if α is big, this means exploration, while small α means exploitation. Here, a chaotic merging factor is used in the merging operation as:

$$X_{\mathrm{k}} = S_2(\cdot) \cdot X'_{\mathrm{k}} + (1 - S_2(\cdot)) \cdot Y_{\mathrm{k}} \tag{16}$$

where $S_2(\cdot)$ is another chaotic ICMIC sequence which is computed as $S_2(r_{\mathrm{k}}) = 0.5 + 0.5 \cdot \sin(\frac{20}{r_{\mathrm{k}}})$. Although ICMIC sequences are employed here, many other chaotic sequences in [41] can also be used. As $S_1(\cdot)$ and $S_2(\cdot)$ are

chaotic sequences with different initial values, they have potential advantage over stochastic sequences by their spread-spectrum characteristic and ergodic properties. So the mutation operation [as Eqs. (13) and (15)] and the merging operation [as Eq. (16)] can have better exploration performance than that of standard ARO [as in Eqs. (10) and (11)].

(c) From simulation and analysis, we also find that the fitness of both larva X'_k and bud X_k sometimes are better than that of parent Y_k, and larva X'_k is better than bud X_k in some cases. The reason is that the larva X'_k is mutated from parent Y_k, and this kind of mutation operation sometimes leads to better solutions. So at each iteration of CARO, the fitness of larva X'_k is also compared with both the parent and the bud. Then, at each iteration of CARO, the fitness of both larva X'_k and bud X_k are compared with the fitness of parent Y_k, and the best fitness of these individuals is chosen to be the survival. This kind of competitive selection between parent, larva, and bud is given by:

$$Y_{k+1} = \begin{cases} X_k, & \text{if} \quad f(X_k) < f(Y_k) \\ X'_k, & \text{if} \quad f(X'_k) < f(Y_k) \\ Y_k, & \text{otherwise} \end{cases} \tag{17}$$

Based on the above analysis, the proposed CARO can be implemented in the following steps, which is also illustrated in Fig. 4.

Step 1 Initialization of CARO parameters: decision variable space $[L, U]$, chaotic sequences $S_1(\cdot)$ and $S_2(\cdot)$, maximum number of iteration k_{max}, iteration number k_1, set iteration number $k = 1$;
Step 2 Compute the fitness of parent Y_k;
Step 3 Generate larva X'_k from parent Y_k, it is a mutation operation as in Eq. (13) or Eq. (15) according to iteration number k_1;
Step 4 Generate bud X_k from larva X'_k and Y_k, it is a kind of merging operation as in Eq. (16);
Step 5 Compute the fitness of bud X_k and larva X'_k;
Step 6 Competitive selection of parent Y_k, bud X_k and larva X'_k based on their fitness values of the optimization problem as in Eq. (17);
Step 7 If stopping conditions are met, stop the CARO; otherwise, $k \leftarrow k + 1$, go to *Step 3*.

4 Simulations

In this section, the performance of the CARO-based parameter extraction technique has been tested. Comparisons with other existing parameter extraction techniques, for different solar cell models, are also conducted. Real measured *V–I* data of solar cell and PV module are

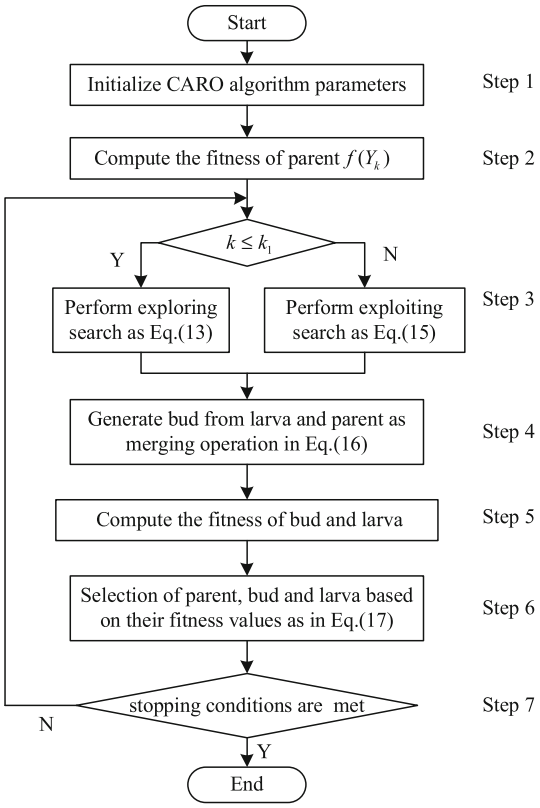

Fig. 4 The flowchart of the proposed CARO

employed in this simulation. The prototype of solar cell is a 57 mm diameter commercial silicon solar cell and the *V–I* measurements have been taken under 1 sun ($1{,}000\,\mathrm{W/m^2}$) at 33 °C. The prototype of PV module is 36 polycrystalline silicon cells which are connected in series and the *V–I* measurements have been taken under 1 sun ($1{,}000\,\mathrm{W/m^2}$) at 45 °C. These two prototypes are the same as in [25–29]. These *V–I* measurements have been widely used by different researchers as benchmark to test electric circuit models and techniques for parameter extraction.

The adjustable parameters of the CARO technique in this simulation, determined by trial, are given by: $k_{max} = 2{,}500, k_1 = 1{,}200$. During the CARO-based optimization process, the lower and upper bounds of optimization parameters X, provided by the literatures [25, 28, 29], are as follows: $R_s(\Omega) \in [0, 0.5]$, $R_{sh}(\Omega) \in [0, 100], I_{ph}(A) \in [0, 1], I_{sd}(\mu A) \in [0, 1]$ and $n \in [1, 2]$.

4.1 Case study 1: double diode model

In this case, 26 pairs *V–I* values as the same as in [6, 24–29] are used as the measured *V–I* data. These measured values are used for the search of optimal parameters vector X^* by the CARO. The convergence process of the CARO during the parameter extraction process for the double

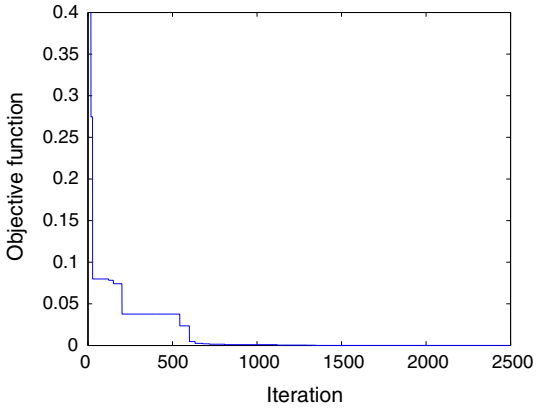

Fig. 5 Convergence process of the CARO for the double diode model

diode model is plotted in Fig. 5, indicating the global optimal value of the objective function as in Eq. (8) during the iterations.

Extracted optimal parameters values X^* and RMSE value for the double diode model by the CARO have been reported in Table 2. Here, CARO has been compared with several other techniques, they are: artificial bee swarm optimization (ABSO) [29], pattern search (PS) [26], simulated annealing (SA) [28], and harmony search algorithm (HSA) [29]. Since it is difficult to test all parameter extraction techniques, these techniques are chosen for comparison because they have been demonstrated with good results for parameter extraction problems. From the comparison results in Table 2, it can be seen that the CARO reaches the lowest RMSE value (9.8260e−4) among these techniques, followed by ABSO, HSA, PS and SA. Since CARO has found the minimum RMSE value, we can know that CARO outperforms ABSO, PS, SA and HSA in this case. As a result, the optimal values X^* found by CARO are closer to the real ones for the double diode model.

Table 2 also indicates that CARO and ABSO rank the overall lowest and second lowest RMSE values among these compared techniques. As the RMSE values of CARO and ABSO are very close, we will compare the results of these two techniques in detail. Two indexes, individual absolute error (IAE) and relative error (RE), are used to show the performance with definition as:

$$\mathrm{IAE} = |I_{\mathrm{measured}} - I_{\mathrm{estimated}}| = |I_{\mathrm{t}} - I'_{\mathrm{t}}| \tag{18}$$

$$\mathrm{RE} = \frac{I_{\mathrm{measured}} - I_{\mathrm{estimated}}}{I_{\mathrm{measured}}} = \frac{I_{\mathrm{t}} - I'_{\mathrm{t}}}{I_{\mathrm{t}}} \tag{19}$$

In Table 3, IAE and RE of each measurement using the optimal values X^* found by CARO and ABSO have been summarized.

In Fig. 6, IAE and RE of each measurement using the optimal values X^* found by CARO and ABSO have been illustrated. From both Fig. 6 and Table 3, we can also know that both CARO and ABSO have very small errors.

In order to illustrate the quality of the extracted optimal values X^* found by CARO, extracted values of $R_{\mathrm{s}}, R_{\mathrm{sh}}, I_{\mathrm{ph}}, I_{\mathrm{sd1}}, I_{\mathrm{sd2}}, n_1$ and n_2 are put into the double diode model in Eq. (2), then the *I–V* and *P–V* characteristic of this model is reconstructed. The *I–V* and *P–V* characteristic resulted from X^* found by CARO along with the real data have been illustrated in Fig. 7. From Fig. 7, we can see that the reconstructed double diode model is in good agreement with the real data.

4.2 Case study 2: single diode model

In this section, the CARO is applied to extract parameters of the single diode model. The 26 pairs real *V–I* values and other conditions are the same as in case 1. The convergence process of the CARO during the parameter extraction process for the single diode model is plotted in Fig. 8, indicating the global optimal value of the objective function as in Eq. (8) during the iterations.

Extracted optimal parameters values X^* and RMSE value for the single diode model by the CARO have been shown in Table 4. Here CARO has been compared with several other techniques, they are: artificial bee swarm optimization (ABSO) [29], chaos particle swarm optimization (CPSO) [24], genetic algorithm (GA) [25], pattern search (PS) [26], simulated annealing (SA) [28], and

Table 2 Comparison among different parameter extraction techniques for the double diode model

Algorithm	CARO	ABSO	PS	SA	HSA
$R_{\mathrm{s}}(\Omega)$	0.03641	0.03657	0.0320	0.0345	0.03545
$R_{\mathrm{sh}}(\Omega)$	54.3967	54.6219	81.3008	43.1034	46.8269
$I_{\mathrm{ph}}(\mathrm{A})$	0.76075	0.76077	0.7602	0.7623	0.76176
$I_{\mathrm{sd1}}(\mu\mathrm{A})$	0.29315	0.26713	0.9889	0.4767	0.12545
$I_{\mathrm{sd2}}(\mu\mathrm{A})$	0.09098	0.38191	0.0001	0.0100	0.25470
n_1	1.47338	1.46512	1.6000	1.5172	1.49439
n_2	1.77321	1.98152	1.1920	2.0000	1.49989
RMSE	9.8260e−4	9.8344e−4	0.01518	0.01664	0.00126

Table 3 IAE and RE of each measurement by CARO and ABSO (double diode model)

			ABSO			CARO		
Meas.	V_t (V)	I_t (A)	I_t'(A)	IAE	RE	I_t'(A)	IAE	RE
1	−0.2057	0.764	0.764031	0.00031	−4.02e−05	0.764026	0.000026	−0.00003
2	−0.1291	0.762	0.762629	0.000629	−0.00083	0.762619	0.000619	−0.00081
3	−0.0588	0.7605	0.761343	0.000843	−0.00111	0.761328	0.000828	−0.00109
4	0.0057	0.7605	0.760162	0.000338	0.000445	0.760141	0.000359	0.00047
5	0.0646	0.76	0.75908	0.00092	0.00121	0.759056	0.000944	0.00124
6	0.1185	0.759	0.758081	0.000919	0.00121	0.758055	0.000945	0.00124
7	0.1678	0.757	0.757139	0.000139	−0.00018	0.757114	0.000114	−0.00015
8	0.2132	0.757	0.756193	0.000807	0.001066	0.756171	0.000829	0.00109
9	0.2545	0.7555	0.755132	0.000368	0.000487	0.755121	0.000379	0.00050
10	0.2924	0.754	0.753694	0.000306	0.000406	0.753696	0.000304	0.00040
11	0.3269	0.7505	0.751392	0.000892	−0.00119	0.751418	0.000918	−0.00122
12	0.3585	0.7465	0.747322	0.000822	−0.0011	0.747370	0.000870	−0.00117
13	0.3873	0.7385	0.740044	0.001544	−0.00209	0.740121	0.001621	−0.00219
14	0.4137	0.728	0.727331	0.000669	0.000919	0.727373	0.000627	0.00086
15	0.4373	0.7065	0.706896	0.000396	−0.00056	0.706955	0.000455	−0.00064
16	0.459	0.6755	0.675265	0.000235	0.000348	0.675261	0.000239	0.00035
17	0.4784	0.632	0.630889	0.001111	0.001758	0.630744	0.001256	0.00198
18	0.496	0.573	0.572114	0.000886	0.001546	0.571923	0.001077	0.00188
19	0.5119	0.499	0.499533	0.000533	−0.00107	0.499610	0.000610	−0.00122
20	0.5265	0.413	0.413525	0.000525	−0.00127	0.413658	0.000658	−0.00159
21	0.5398	0.3165	0.31723	0.00073	−0.00231	0.317521	0.001021	−0.00322
22	0.5521	0.212	0.21209	0.00009	−0.00042	0.212162	0.000162	−0.00076
23	0.5633	0.1035	0.102694	0.000806	0.007788	0.102753	0.000747	0.00721
24	0.5736	−0.01	−0.00927	0.00073	0.07253	−0.009278	0.000722	0.07216
25	0.5833	−0.123	−0.12439	0.00139	−0.01126	−0.124355	0.001355	−0.01101
26	0.59	−0.21	−0.20917	0.00083	0.003965	−0.209207	0.000793	0.00377

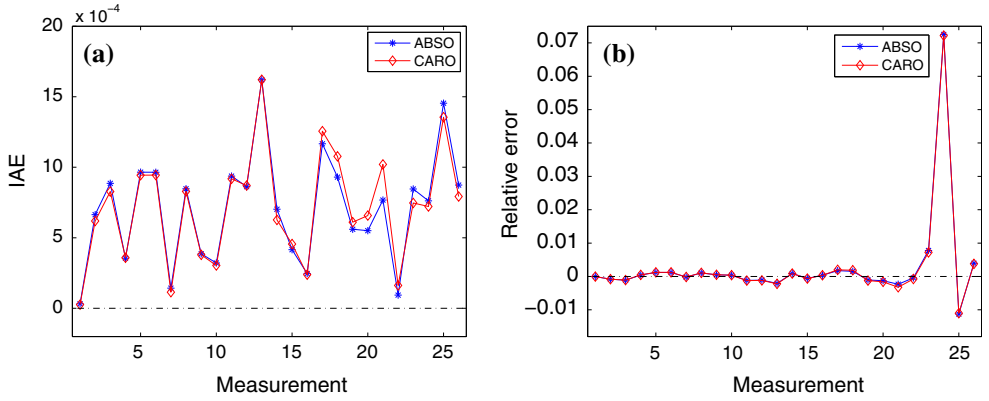

Fig. 6 IAE and RE of each measurement by CARO and ABSO (double diode model). **a** Individual absolute error, **b** relative error

harmony search algorithm (HSA) [29]. From the comparison results in Table 4, we can see that the CARO provides the lowest RMSE value (9.8665e−4) among these techniques, followed by ABSO, HSA, CPSO, PS, SA and GA. Since CARO has found the minimum RMSE value, we can know that CARO outperforms ABSO, CPSO, GA, PS, SA and HSA in this case. As a result, the optimal values X^* found by CARO are closer to the real ones for the single diode model.

Table 4 also indicates that CARO and ABSO rank the overall lowest and second lowest RMSE values among these compared techniques. As the RMSE values of CARO

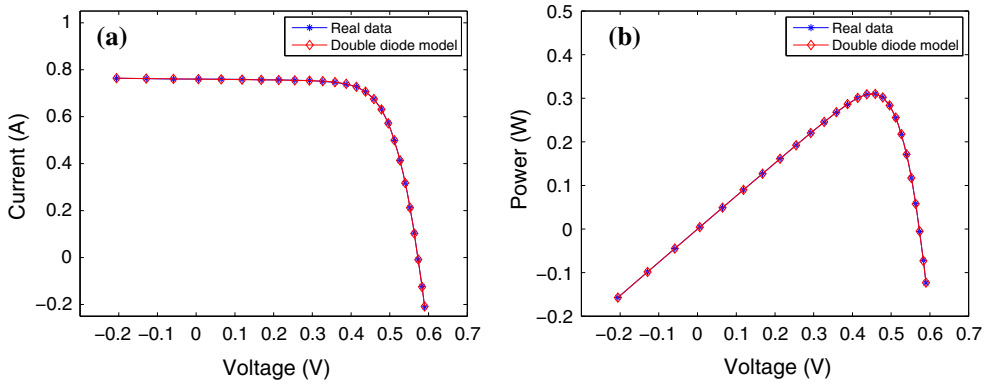

Fig. 7 Comparison results from the real data and the double diode model. **a** *I–V* characteristics, **b** *P–V* characteristics

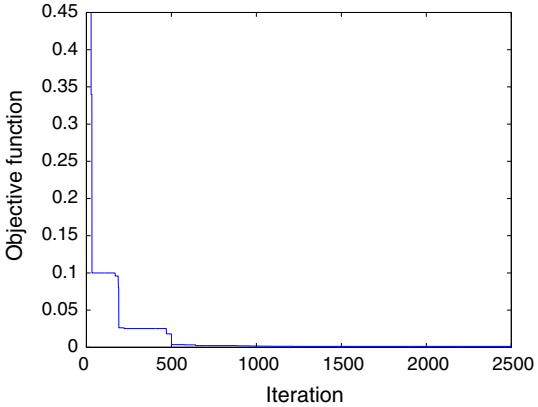

Fig. 8 Convergence process of the CARO for the single diode model

and ABSO are very close, we will compare the results of these two techniques in detail. Two indexes, IAE and RE, are also used to show the performance.

In Table 5, IAE and RE of each measurement using the optimal values X^* found by CARO and ABSO have been summarized. In Table 5, IAE and RE of each measurement using the optimal values X^* found by CARO and ABSO have been calculated. Figure 9 illustrates the IAE and RE of each measurement using the optimal values X^* found by CARO and ABSO. From both Fig. 9 and Table 5, we can also know that both CARO and ABSO have very small errors.

In order to illustrate the quality of the extracted optimal values X^* found by CARO, extracted values of $R_s, R_{sh}, I_{ph}, I_{sd}$ and n are put into the single diode model in Eq. (3), then the *I–V* and *P–V* characteristic of the single diode model is reconstructed. The *I–V* and *P–V* characteristic resulted from extracted optimal values X^* by CARO along with the real data have been illustrated in Fig. 10. From Fig. 10, we can see that the reconstructed double diode model is in good agreement with the real data.

4.3 Case study 3: PV module

In this case, real *V–I* values of PV module as the same as in [24, 25, 27, 28, 42, 43] are used as the measurements, which are derived from a 36 polycrystalline silicon cells which are connected in series under 1 sun (1,000 W/m^2) at 45 °C. In this simulation, these measured values are used to extract the PV model parameters by the CARO.

Extracted optimal parameters values X^* and RMSE value for the PV module by the CARO have been reported in Table 6. Here, CARO is also compared with several other techniques, they are: Newton [7], method in [42], CPSO [24], method in [43], PS [25] and SA [28].

The comparison among different parameter extraction techniques for the PV module has been summarized in Table 6. It can seen from Table 6 that like the previous cases, CARO also gets the lowest RMSE value (0.002427)

Table 4 Comparison among different parameter extraction techniques for the single diode model

Algorithm	CARO	ABSO	CPSO	GA	PS	SA	HSA
$R_s(\Omega)$	0.03644	0.03659	0.0354	0.0299	0.0313	0.0345	0.03663
$R_{sh}(\Omega)$	53.0893	52.2903	59.012	42.3729	64.1026	43.1034	53.5946
I_{ph} (A)	0.76079	0.76080	0.7607	0.7619	0.7617	0.7620	0.76070
$I_{sd}(\mu A)$	0.31724	0.30623	0.4000	0.8087	0.9980	0.4798	0.30495
n	1.48168	1.47878	1.5033	1.5751	1.6000	1.5172	1.47538
RMSE	9.8665e-4	9.9124e-4	0.00139	0.01908	0.01494	0.01900	9.9510e-4

Table 5 IAE and RE of each measurement by CARO and ABSO (single diode model)

			ABSO			CARO		
Meas.	V_t (V)	I_t (A)	I_t'(A)	IAE	RE	I_t'(A)	IAE	RE
1	−0.2057	0.764	0.764201	0.000201	−0.00026	0.764023	0.000023	−0.00003
2	−0.1291	0.762	0.762737	0.000737	−0.00097	0.762610	0.000610	−0.00080
3	−0.0588	0.7605	0.761393	0.000893	−0.00117	0.761313	0.000813	−0.00107
4	0.0057	0.7605	0.76016	0.00034	0.000447	0.760121	0.000379	0.00049
5	0.0646	0.76	0.759032	0.000968	0.001274	0.759031	0.000969	0.00127
6	0.1185	0.759	0.757992	0.001008	0.001328	0.758026	0.000974	0.00128
7	0.1678	0.757	0.757017	0.000017	−2.21e−05	0.757082	0.000082	−0.00011
8	0.2132	0.757	0.756047	0.000953	0.001259	0.756139	0.000861	0.00114
9	0.2545	0.7555	0.754977	0.000523	0.000692	0.755091	0.000409	0.00054
10	0.2924	0.754	0.753547	0.000453	0.0006	0.753674	0.000326	0.00043
11	0.3269	0.7505	0.751277	0.000777	−0.00103	0.751408	0.000908	−0.00121
12	0.3585	0.7465	0.74726	0.00076	−0.00102	0.747378	0.000878	−0.00118
13	0.3873	0.7385	0.740051	0.001551	−0.0021	0.740149	0.001649	−0.00223
14	0.4137	0.728	0.727411	0.000589	0.000809	0.727421	0.000579	0.00079
15	0.4373	0.7065	0.707033	0.000533	−0.00076	0.707016	0.000516	−0.00073
16	0.459	0.6755	0.675431	0.000069	0.000102	0.675325	0.000175	0.00026
17	0.4784	0.632	0.631046	0.000954	0.001509	0.630799	0.001201	0.00190
18	0.496	0.573	0.57223	0.00077	0.001344	0.571959	0.001041	0.00182
19	0.5119	0.499	0.499591	0.000591	−0.00118	0.499622	0.000622	−0.00125
20	0.5265	0.413	0.413524	0.000524	−0.00127	0.413646	0.000646	−0.00157
21	0.5398	0.3165	0.317184	0.000684	−0.00216	0.317192	0.000692	−0.00219
22	0.5521	0.212	0.212023	0.000023	−0.00011	0.212126	0.000126	−0.00059
23	0.5633	0.1035	0.10263	0.00087	0.008404	0.102621	0.000879	0.00849
24	0.5736	−0.01	−0.00931	0.00069	0.068809	−0.009415	0.000585	0.05847
25	0.5833	−0.123	−0.12438	0.00138	−0.01118	−0.124350	0.001350	−0.01097
26	0.59	−0.21	−0.20911	0.00089	0.00423	−0.209138	0.000862	0.00410

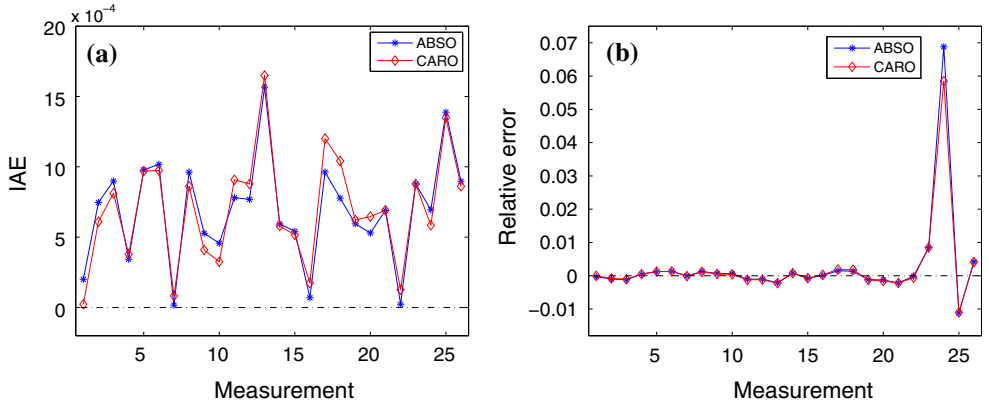

Fig. 9 IAE and RE of each measurement by CARO and ABSO (single diode model). **a** Individual absolute error, **b** relative error

among these techniques, followed by SA, CPSO, method in [43], PS, method in [42] and Newton. Since CARO has found the minimum RMSE value in the parameter extraction of the PV module, we can know that CARO outperforms SA, CPSO, method in [43], PS, method in [42] and Newton in this case.

Table 7 and Fig. 11 have also summarized the IAE of each measurement using the extracted optimal parameters values X^* found by CARO, Newton [7], PS [25], method in [42] and SA [28]. The total IAE, which is the summarize of IAE for each measurement, is also computed in Table 7. The results in Table 7 also indicate that the extracted

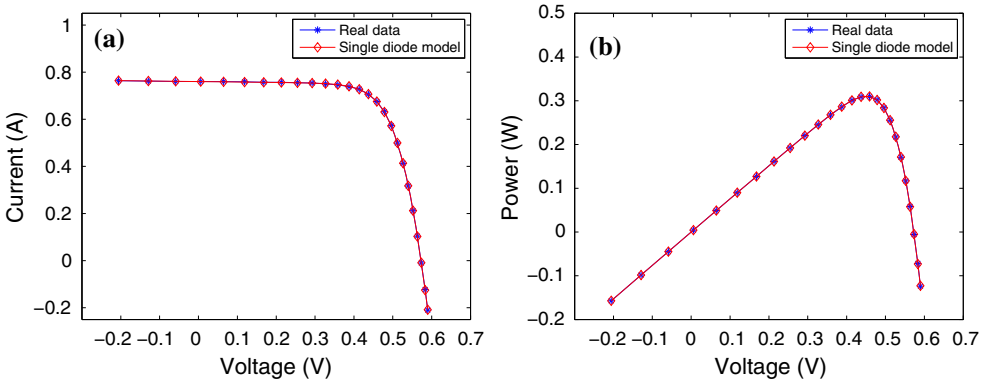

Fig. 10 Comparison results from the real data and the single diode model. **a** *I–V* characteristics, **b** *P–V* characteristics

Table 6 Comparison among different parameter extraction techniques for the PV module

Algorithm	CARO	Newton	Ref. [42]	CPSO	Ref. [43]	PS	SA
I_{ph} (A)	1.03185	1.0318	1.0339	1.0286	1.0310	1.0313	1.0331
I_{sd} (μA)	3.28401	3.2875	3.0760	8.3010	3.8236	3.1756	3.6642
R_s (Ω)	1.20556	1.2057	1.2030	1.0755	1.0920	1.2053	1.1989
R_{sh} (Ω)	841.3213	555.5556	555.5556	1,850.1000	689.6600	714.2857	833.3333
n	48.40363	48.4500	48.1862	52.2430	48.9300	48.2889	48.8211
RMSE	0.002427	0.7805	0.6130	0.0035	0.0102	0.0118	0.0027

Table 7 IAEs of each measurement by different techniques (PV module)

Meas.	V_t (V)	I_t (A)	CARO	Newton	PS	Ref. [42]	SA
1	0.1248	1.0315	0.00129	0.00213	0.00220	0.00008	0.00006
2	1.8093	1.0300	0.00178	0.00303	0.00378	0.00165	0.00064
3	3.3511	1.0260	0.00049	0.00127	0.00265	0.00050	0.00141
4	4.7622	1.0220	0.00250	0.00056	0.00141	0.00077	0.00349
5	6.0538	1.0180	0.00257	0.00226	0.00024	0.00197	0.00541
6	7.2364	1.0155	0.00370	0.00199	0.00101	0.00124	0.00529
7	8.3189	1.0140	0.00215	0.00042	0.00388	0.00155	0.00296
8	9.3097	1.0100	0.00094	0.00253	0.00642	0.00399	0.00083
9	10.2163	1.0035	0.00379	0.00602	0.01032	0.00772	0.00282
10	11.0449	0.9880	0.00435	0.00660	0.01126	0.00844	0.00370
11	11.8018	0.9630	0.00411	0.00650	0.01145	0.00837	0.00403
12	12.4929	0.9255	0.00275	0.00544	0.01059	0.00722	0.00350
13	13.1231	0.8725	0.00081	0.00235	0.00756	0.00393	0.00100
14	13.6983	0.8075	0.00084	0.00231	0.00742	0.00360	0.00152
15	14.2221	0.7265	0.00107	0.00012	0.00471	0.00082	0.00044
16	14.6995	0.6345	0.00136	0.00125	0.00309	0.00068	0.00122
17	15.1346	0.5345	0.00129	0.00062	0.00307	0.00040	0.00036
18	15.5311	0.4275	0.00158	0.00115	0.00173	0.00126	0.00080
19	15.8929	0.3185	0.00027	0.00039	0.00234	0.00001	0.00074
20	16.2229	0.2085	0.00077	0.00161	0.00255	0.00103	0.00189
21	16.5241	0.1010	0.00124	0.00521	0.00505	0.00448	0.00534
22	16.7987	−0.0080	0.00045	0.00056	0.00067	0.00023	0.00059
23	17.0499	−0.1110	0.00042	0.00005	0.00228	0.00075	0.00006
24	17.2793	−0.2090	0.00048	0.00024	0.00319	0.00052	0.00000
25	17.4885	−0.3030	0.00091	0.00227	0.00675	0.00296	0.00262
Total IAE			0.04197	0.05688	0.11561	0.06418	0.05071

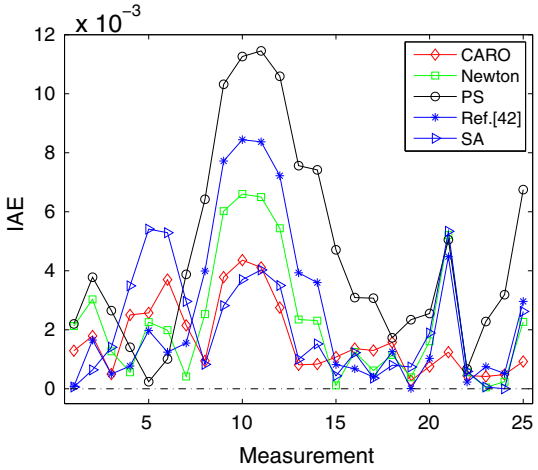

Fig. 11 IAE of each measurement by different techniques (PV module)

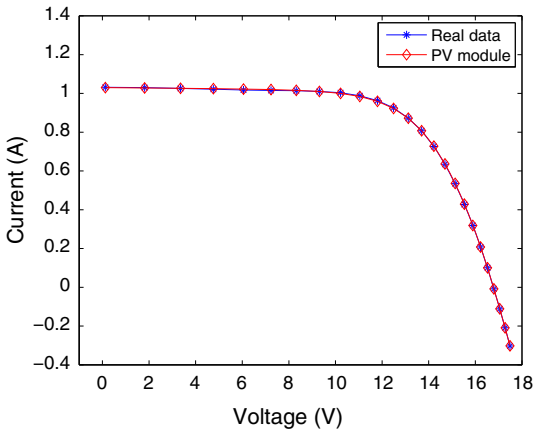

Fig. 12 Comparison results from the real data and the PV module

optimal parameters values X^* found by CARO gets the lowest total-IAE value (0.04197) among these techniques for the PV module. The simulation results in Table 7 and Fig. 11 show that CARO outperforms Newton, PS, method in [42] and SA in this parameter extraction simulation.

In order to illustrate the quality of the extracted optimal values X^* found by CARO, X^* is used to reconstruct *I–V* characteristic of the PV module, and the reconstructed *I–V* characteristic is illustrated in Fig. 12. According the *I–V* characteristic shown in Fig. 12, we can know that the reconstructed *I–V* characteristic using extracted optimal values found by CARO fit the real data very well.

From these three simulation cases (Case 1, Case 2, Case 3) for different solar cell models, the proposed CARO technique has found the lowest RMSE value among the compared techniques. The computation cost of optimization algorithm is another aspect in simulation. The CARO is a kind of individual-based optimization algorithm, while ABSO, CPSO, GA and HSA are population-based optimization algorithm. Generally speaking, individual-based optimization algorithm shows small computation cost. As a result, the computation cost of CARO is smaller than that of population-based optimization algorithm. Since the parameter extraction of solar cell models is not a real-time optimization problem, the computation cost is not a limit for optimization algorithm. Therefore, the proposed CARO technique shows superiority over several meta-heuristic algorithms, such as GA, CPSO, ABSO, SA, PS and HSA, for the parameter extraction of solar cell models.

5 Conclusion

This paper proposes a novel CARO technique for the parameter extraction of solar cell models. As an improvement to original ARO, the proposed CARO employs chaotic sequence to enhance its global optimization ability. Then, the CARO provides a good balance between exploration and exploitation. The parameter extraction of solar cell models is formalized as a optimization problem, which establishes an objective function minimizing the errors between the estimated and measured data. All the 7 or 5 parameters of solar cell models are extracted simultaneously using measured input–output data. In the simulation, the CARO is applied to extract the parameters of different solar cell models, i.e., double diode, single diode, and PV module. Comparison results with other meta-heuristic algorithms, such as GA, CPSO, ABSO, SA, PS and HSA, show that the CARO reaches the lowest errors. The CARO is a kind of individual-based optimization algorithm, so it also shows small computation cost. The proposed new technique provides another optional method to extract parameters of solar cell models.

References

1. Liu GY, Nguang SK, Partridge A (2011) A general modeling method for I–V characteristics of geometrically and electrically configured photovoltaic arrays. Energy Convers Manag 52(12):3439–3445
2. Amrouche B, Guessoum A, Belhamel M (2012) A simple behavioural model for solar module electric characteristics based on the first order system step response for MPPT study and comparison. Appl Energy 91(1):395–404
3. Khan F, Baek SH, Park Y, Kim JH (2013) Extraction of diode parameters of silicon solar cells under high illumination conditions. Energy Convers Manag 76:421–429
4. Orioli A, Gangi AD (2013) A procedure to calculate the five-parameter model of crystalline silicon photovoltaic modules on the basis of the tabular performance data. Appl Energy 102(SI):1160–1177

5. Tian HM, Mancilla-David F, Ellis K, Muljadi E, Jenkins P (2012) A cell-to-module-to-array detailed model for photovoltaic panels. Sol Energy Mater Sol Cells 86(9):2695–2706
6. Cubas J, Pindado S, Victoria M (2014) On the analytical approach for modeling photovoltaic systems behavior. J Power Sources 247:467–474
7. Easwarakhanthan T, Bottin J, Bouhouch I, Boutrit C (1986) Nonlinear minimization algorithm for determining the solar cell parameters with microcomputers. Sol Energy 4(1):1–12
8. Kim W, Choi W (2010) A novel parameter extraction method for the one-diode solar cell model. Sol Energy 84(6):1008–1019
9. Das AK (2012) Analytical derivation of explicit J–V model of a solar cell from physics based implicit model. Sol Energy 86(1):26–30
10. Lun SX, Du CJ, Yang GH, Wang S, Guo TT, Sang JS, Li JP (2013) An explicit approximate I–V characteristic model of a solar cell based on pad*é* approximants. Sol Energy 92:147–159
11. Lun SX, Du CJ, Guo TT, Wang S, Sang JS, Li JP (2013) A new explicit I–V model of a solar cell based on Taylor's series expansion. Sol Energy 94:221–232
12. Bayhan H, Bayhan M (2011) A simple approach to determine the solar cell diode ideality factor under illumination. Sol Energy 85(5):769–775
13. Ghani F, Duke M, Carson J (2013) Numerical calculation of series and shunt resistance of a photovoltaic cell using the Lambert W-function: experimental evaluation. Sol Energy 87:246–253
14. Ghani F, Duke M, Carson J (2013) Numerical calculation of series and shunt resistances and diode quality factor of a photovoltaic cell using the Lambert *W*-function. Sol Energy 91:422–431
15. Chen YF, Wang XM, Li D, Hong RJ, Shen H (2011) Parameters extraction from commercial solar cells I–V characteristics and shunt analysis. Appl Energy 88(6):2239–2244
16. Peng LL, Sun YZ, Meng Z, Wang YL, Xu Y (2013) A new method for determining the characteristics of solar cells. J Power Sources 227:131–136
17. Karatepe E, Boztepe M, Colak M (2006) Neural network based solar cell model. Energy Convers Manag 47(9-10):1159–1178
18. Patra JC (2011) Neural network-based model for dual-junction solar cells. Progress in Photovoltaics 19(1):33–44
19. Patra JC (2011) Chebyshev neural network-based model for dual-junction solar cells. IEEE Trans Energy Convers 26(1):132–139
20. Fathabadi H (2013) Novel neural-analytical method for determining silicon/plastic solar cells and modules characteristics. Energy Convers Manag 76:253–259
21. Bonanno F, Capizzi G, Graditi G, Napoli C, Tina GM (2012) A radial basis function neural network based approach for the electrical characteristics estimation of a photovoltaic module. Appl Energy 97(SI):956–961
22. Zagrouba M, Sellami A, Bouaicha M, Ksouri M (2010) Identification of PV solar cells and modules parameters using the genetic algorithms: application to maximum power extraction. Sol Energy 84(5):860–866
23. Ye M, Wang X, Xu Y (2009) Parameter extraction of solar cells using particle swarm optimization. J Appl Phys 105(9):094502
24. Huang W, Jiang C, Xue L, Song D (2011) Extracting solar cell model parameters based on chaos particle swarm algorithm. In: Proceedings of international conference on electric information and control engineering (ICEICE), pp 398–402
25. AlRashidi MR, AlHajri MF, El-Naggar KM, Al-Othman AK (2011) A new estimation approach for determining the I–V characteristics of solar cells. Sol Energy 85(7):1543–1550
26. AlHajri MF, El-Naggar KM, AlRashidi MR, Al-Othman AK (2012) Optimal extraction of solar cell parameters using pattern search. Renew Energy 44:238–245
27. Gong W, Cai Z (2013) Parameter extraction of solar cell models using repaired adaptive differential evolution. Sol Energy 94:209–220
28. El-Naggar KM, AlRashidi MR, AlHajri MF, Al-Othman AK (2012) Simulated Annealing algorithm for photovoltaic parameters identification. Sol Energy 86(1):266–274
29. Askarzadeh A, Rezazadeh A (2013) Artificial bee swarm optimization algorithm for parameters identification of solar cell models. Appl Energy 102(SI):943–949
30. Farasat A, Menhaj MB, Mansouri T, Moghadam MRS (2010) ARO: a new model-free optimization algorithm inspired from asexual reproduction. Appl Soft Comput 10(4):1284–1292
31. Mansouri T, Farasat A, Menhaj MB, Moghadam MRS (2011) ARO: a new model free optimization algorithm for real time applications inspired by the asexual reproduction. Expert Syst Appl 38(5):4866–4874
32. Khanteymoori AR, Menhaj MB, Homayounpour MM (2011) Structure learning in Bayesian networks using asexual reproduction optimization. ETRI J 33(1):39–49
33. Asl AN, Menhaj MB, Sajedin A (2014) Control of leader–follower formation and path planning of mobile robots using Asexual Reproduction Optimization (ARO). Appl Soft Comput 14:563–576
34. Yuan XF, Yang YM, Wang H (2012) Improved parallel chaos optimization algorithm. Appl Math Comput 219(8):3590–3599
35. Tatsumi K, Ibuki T, Tanino T (2013) A chaotic particle swarm optimization exploiting a virtual quartic objective function based on the personal and global best solutions. Appl Math Comput 219(17):8991–9011
36. Yang DX, Liu ZJ, Zhou JL (2014) Chaos optimization algorithms based on chaotic maps with different probability distribution and search speed for global optimization. Commun Nonlinear Sci Numer Simul 19(4):1229–1246
37. Ma S (2012) Chaotic populations in genetic algorithm. Appl Soft Comput 12(8):2409–2424
38. Li Y, Wen Q, Zhang B (2012) Chaotic ant swarm optimization with passive congregation. Nonlinear Dyn 68(1-2):129–136
39. Gao SC, Vairappan C, Wang Y, Cao QP, Tang Z (2014) Gravitational search algorithm combined with chaos for unconstrained numerical optimization. Appl Math Comput 231:48–62
40. Alatas B (2010) Chaotic harmony search algorithms. Appl Math Comput 216(9):2687–2699
41. Baykasoglu Adil (2012) Design optimization with chaos embedded great deluge algorithm. Appl Soft Comput 12(3):1055–1067
42. Bouzidi K, Chegaar M, Nehaoua N (2007) New method to extract the parameters of solar cells from their illuminated I–V curve. In: 4th international conference on computer integrated manufacturing
43. Chegaar M, Nehaoua N, Bouhemadou A (2008) Organic and inorganic solar cells parameters evaluation from single I–V plot. Energy Convers Manag 49(6):1376–1379